

1 Reconstruction of a daily gridded snow water equivalent product for 2 the land region above 45° N based on a ridge regression machine 3 learning approach

4 Donghang Shao^{1,2}, Hongyi Li^{1,2}, Jian Wang^{1,2,4}, Xiaohua Hao^{1,2}, Tao Che^{1,2} and Wenzheng Ji^{1,2,3}

5 ¹Heihe Remote Sensing Experimental Research Station, Northwest Institute of Eco-Environment and Resources, Chinese
6 Academy of Sciences, Lanzhou 730000, China

7 ²Key Laboratory of Remote Sensing of Gansu Province, Northwest Institute of Eco-Environment and Resources, Chinese
8 Academy of Sciences, Lanzhou 730000, China

9 ³University of Chinese Academy of Sciences, Beijing 100049, China

10 ⁴Jiangsu Center for Collaborative Innovation in Geographical Information Resource Development and Application, Nanjing
11 210023, China

12 *Correspondence to:* Hongyi Li (lihongyi@lzb.ac.cn)

13 **Abstract.** The snow water equivalent (SWE) is an important parameter of surface hydrological and climate systems, and it
14 has a profound impact on Arctic amplification and climate change. However, there are great differences among existing SWE
15 products. In the land region above 45° N, the existing SWE products are associated with a limited time span and limited
16 spatial coverage, and the spatial resolution is coarse, which greatly limits the application of SWE data in cryosphere change
17 and climate change studies. In this study, utilizing the ridge regression model (RRM) of a machine learning algorithm, we
18 integrated various existing SWE products to generate a spatiotemporally seamless and high-precision RRM SWE product.
19 The results show that it is feasible to utilize a ridge regression model based on a machine learning algorithm to prepare SWE
20 products on a global scale. We evaluated the accuracy of the RRM SWE product using hemispheric-scale snow course
21 (HSSC) observational data and Russian snow survey data. The MAE, RMSE, R, and R² between the RRM SWE products
22 and observed SWEs are 0.21, 25.37 mm, 0.89, and 0.79, respectively. The accuracy of the RRM SWE dataset is improved by
23 28%, 22%, 37%, 11%, and 11% compared with the original AMSR-E/AMSR2 (SWE), ERA-Interim SWE, Global Land
24 Data Assimilation System (GLDAS) SWE, GlobSnow SWE, and ERA5-land SWE datasets, respectively, and it has a higher

25 spatial resolution. The RRM SWE product production method does not rely heavily on an independent SWE product; it takes
26 full advantage of each SWE dataset, and it takes into consideration the altitude factor. The MAE ranges from 0.16 for areas
27 within <100 m elevation to 0.29 within the 800-900 m elevation range. The MAE is best in the Russian region and worst in
28 the Canadian region. The RMSE ranges from 4.71 mm for areas within <100 m elevation to 31.14 mm within the >1000 m
29 elevation range. The RMSE is best in the Finland region and worst in the Canadian region. This method has good stability, is
30 extremely suitable for the production of snow datasets with large spatial scales, and can be easily extended to the preparation
31 of other snow datasets. The RRM SWE product is expected to provide more accurate SWE data for the hydrological model
32 and climate model and provide data support for cryosphere change and climate change studies. The RRM SWE product is
33 available from ‘A Big Earth Data Platform for Three Poles’ (<http://dx.doi.org/10.11888/Snow.tpd.271556>) (Li et al., 2021).

34 **1 Introduction**

35 The IPCC (Intergovernmental Panel on Climate Change) AR6 (Sixth Assessment Report) notes that the Northern
36 Hemisphere spring snow cover has greatly decreased since 1950, and the feedback effect of the climate system caused by
37 this reduction is extremely large (Masson-Delmotte et al., 2021). In most land areas of the Northern Hemisphere, annual
38 runoff is dominated by snowmelt, and accurately estimating the impacts of such a large amount of snowmelt runoff on
39 ecosystems and human activities is of great significance (Barnett et al., 2005; Bintanja and Andry, 2017; Henderson et al.,
40 2018). Whether through hydrometeorological simulation or global change research, the estimation of the energy budget and
41 mass of snow is very difficult, so a set of highly accurate, long time series snow cover datasets is urgently needed to drive
42 hydrometeorological simulations and land surface process models. Among them, snow water equivalent (SWE) data play an
43 irreplaceable role as an important parameter of the land surface hydrological model and climate model.

44 At present, there are many forms of SWE data in the world. According to type, these data can be divided into site
45 observational SWE, remote sensing SWE, reanalysis SWE, data assimilation SWE and model simulation SWE. The remote
46 sensing SWEs are mainly AMSR-E (Kelly, 2009) and AMSR2 (Imaoka et al., 2010; Tedesco and Jeyaratnam, 2019). The
47 reanalysis SWE was mainly based on the ERA-Interim (Dee et al., 2011), MERRA2 (Gelaro et al., 2017), MERRA land

48 (Reichle et al., 2011), and ERA5-land (Muñoz Sabater, 2019; Balsamo et al., 2015) datasets. The data assimilation SWE
49 mainly includes GlobSnow (Luoju et al., 2021) and the Global Land Data Assimilation System (GLDAS) (Rodell et al.,
50 2004). The site observational SWE mainly includes the GHCN dataset (Menne et al., 2016) and HSSC data (Pulliainen et al.,
51 2020). However, the time ranges of AMSR-E and AMSR-E2 SWE are only from 2003 to the present, which is lacking in
52 terms of time series. Similarly, the GlobSnow SWE dataset is also seriously lacking in time series. Although the reanalysis
53 SWE data have good spatial and temporal continuity and high data integrity, their accuracy is poor, and the MAE is 0.65
54 (Snauffer et al., 2016). The SWE data from stations and meteorological observations cannot meet the needs of
55 hydrometeorological and climate change research. This is mainly because SWE from stations is discontinuous in time series
56 and severely missing. Furthermore, hydrometeorological studies often require spatiotemporally continuous grid data to be
57 derived (Pan et al., 2003). There are great differences among remote-sensing SWE, reanalysis SWE data, data assimilation
58 SWE and observational SWE. For remote-sensing SWE, the spatiotemporal characteristics of different passive microwave
59 SWE data differ significantly due to differences in sensors or retrieval algorithms (Mudryk et al., 2015a). Data assimilation
60 SWE and reanalysis SWE data also tend to exhibit different spatiotemporal characteristics due to differences in model
61 design, driving data, and assimilation methods (Vuyovich et al., 2014). In summary, although there are a variety of SWE data
62 in the world, the data quality is uncertain.

63 Previous studies have shown that all kinds of SWE data in the Northern Hemisphere have advantages and disadvantages,
64 and none of these data perform well in all aspects (Mortimer et al., 2020). An effective method was applied in a study by
65 Pulliainen et al. (Pulliainen et al., 2020), who applied a bias correction to GlobSnow and reanalysis data products based on
66 SWE snow course measurements to obtain improved estimates on annual peak snow mass and SWE in the Northern
67 Hemisphere. Another effective method is to fuse all kinds of SWE data in time and space, integrate the advantages of all
68 kinds of data, and then generate a relatively complete SWE dataset. Many scholars have conducted in-depth studies on SWE
69 data fusion. The main fusion methods can be classified into the following categories: multiproduct direct averaging (Mudryk
70 et al., 2015b), linear regression (Snauffer et al., 2016), data assimilation (Pulliainen, 2006), “multiple” collocation (Pan et al.,
71 2015) and machine learning (Snauffer et al., 2018; Xiao et al., 2018; Wang et al., 2020). Studies have shown that even the
72 simplest multisource data average is more accurate than a single SWE product (Snauffer et al., 2018). However, the simple

73 multisource data average cannot highlight the advantages of high-precision data, and it is easily affected by the weight ratio
74 of low-precision data, which reduces the accuracy of fused data (Mudryk et al., 2015a). Although the linear regression
75 method can make good use of the actual observational data to correct the original data, it is easy to overfit and causes the
76 overall deviation (Snauffer et al., 2016). The “multiple” collocation method changes the size of the original SWE data before
77 fusion, which easily causes data errors. The data assimilation method is sensitive to the accuracy of input data, and it is
78 difficult to fuse multisource data (Pan et al., 2015). In recent years, machine learning methods have been widely used in data
79 fusion (Santi et al., 2021; Ntokas et al., 2021). Machine learning methods can not only integrate the advantages of
80 multisource data but also make full use of site observational data to train the sample data, which easily generates SWE data
81 products with large spatial scales and long time series (Broxton et al., 2019; Bair et al., 2018).

82 In summary, based on the existing SWE data products, combining a machine learning algorithm to fuse multisource SWE
83 data is an effective method to prepare SWE products with long time series and large spatial scales and retain the advantages
84 of single SWE data products. The ridge regression model is a biased estimation method specifically designed to address the
85 problem of multicollinear data (Duzan and Shariff, 2015; Saleh et al., 2019). It has good tolerance to "ill-conditioned" data
86 and has a good effect in using SWE data to address the multicollinearity problem (Hoerl and Kennard, 1970b; Guilkey and
87 Murphy, 1975). In this study, we integrated multisource SWE data products of the RRM SWE based on the ridge regression
88 model of the machine learning algorithm. We selected ERA-Interim SWE, GLDAS SWE, GlobSnow SWE, AMSR-
89 E/AMSR2 SWE, and ERA5-land SWE data with relatively complete time series as the original data for the production of the
90 RRM SWE product. The missing parts of the ERA-Interim SWE, AMSR-E/AMSR2 SWE, and GlobSnow SWE data were
91 filled by the spatiotemporal interpolation method. The HSSC dataset (Pulliainen et al., 2020) and Russian snow survey data
92 (Bulygina et al., 2011) were used as training sample data of "true SWE", and the effect of altitude on the algorithm was also
93 considered. Thus, we prepared a set of spatiotemporal seamless SWE datasets (RRM SWE) covering the land region above
94 45° N from 1979 to 2019. The spatial coverage of the RRM SWE product covers all land regions north of 45° N.

95 **2 Data and methods**

96 **2.1 Research region**

97 The research region of the RRM SWE product is located in the land region north of 45° N (Fig. 1). This region consists of
98 Asia, Europe, and North America. The land region covers Russia, the United States, Canada, Denmark, Norway, Iceland,
99 Sweden, and Finland. This region has a cold climate and a wide area of snow cover.

100 **2.2 Grid SWE data description**

101 In this study, we utilized ERA-Interim SWE data (Dee et al., 2011), GLDAS SWE data (Rodell et al., 2004), GlobSnow
102 SWE data (Luoju et al., 2021), AMSR-E/AMSR2 SWE data (Tedesco and Jeyaratnam, 2019), and ERA5-land SWE data
103 (Muñoz Sabater, 2019) as the original input datasets for the fusion data (Table 1).

104 GlobSnow is a dataset of global snow cover and SWEs for the Northern Hemisphere released by the European Space
105 Agency (ESA) (<http://www.globsnow.info/swe/>) (Luoju et al., 2021; Pulliainen et al., 2020). The SWE products in this
106 dataset combine the Canadian Meteorological Center (CMC) daily snow depth analysis data (Walker et al., 2011), ground
107 weather site observational data, and satellite microwave radiometer data. We obtained the L3A_daily_SWE product of this
108 dataset. The temporal resolution of the L3A_daily_SWE product is daily, the spatial resolution is 0.25°, and the data format
109 is NETCDF4.

110 ERA-Interim is the fourth generation reanalysis data of the European Centre for Medium-Range Weather Forecasts
111 (ECMWF) (Dee et al., 2011). The data provide a global assimilated numerical product of various surface and top
112 atmospheric parameters from January 1979 to the present ([https://apps.ecmwf.int/datasets/data/interim-full-
113 daily/levtype=sfc/](https://apps.ecmwf.int/datasets/data/interim-full-daily/levtype=sfc/)). We obtained the SWE dataset with a daily temporal resolution, a spatial resolution of 0.25°, and
114 NETCDF4 data format. The spatial range of the data is the land region above 45° N.

115 The Advanced Microwave Scanning Radiometer-Earth Observation System (AMSR-E) is a microwave scanning
116 radiometer on the Aqua satellite of the National Aeronautics and Space Administration (NASA) Earth Observation System
117 (EOS) (Tedesco and Jeyaratnam, 2019). The AMSR-E provides a global daily SWE dataset from June 19, 2002, to October

118 3, 2011 (https://nsidc.org/data/ae_dysno). AMSR2 is a microwave scanning radiometer on the GCOM-W1 satellite launched
119 by the Japan Aerospace Exploration Agency (JAXA) in May 2012. AMSR2 provides a global SWE dataset from July 2,
120 2012, to the present (https://nsidc.org/data/AU_DySno/versions/1). The spatial resolution of the AMSR-E SWE and AMSR2
121 SWE datasets is 25 km x 25 km, the temporal resolution is daily, and the data formats are HDF-EOS and HDF-EOS5,
122 respectively.

123 The GLDAS is a model used to describe global land information; it contains data, such as global rainfall, water
124 evaporation, surface runoff, underground runoff, soil moisture, surface snow cover distribution, temperature, and heat flow
125 distribution (Rodell et al., 2004). This assimilation system includes data with spatial resolutions of $1^{\circ} \times 1^{\circ}$ and $0.25^{\circ} \times 0.25^{\circ}$
126 and temporal resolutions of 3 hours, 1 day and 1 month. The GLDAS data are available for download from the Goddard
127 Earth Sciences Data and Information Services Center (GES DISC). We obtain an SWE dataset with a daily temporal
128 resolution, 0.25° spatial resolution, and NETCDF4 data format.

129 ERA5-land is a reanalysis dataset that provides the evolution of global land parameter data since 1981 (Muñoz Sabater,
130 2019). The dataset provides eight types of snow parameter data, including snow albedo, snow cover, snow depth, snowfall,
131 the temperature of the snow layer, snowmelt, snow density, and SWE. This dataset provides a global SWE dataset with an
132 hourly spatial resolution, a temporal resolution of $0.1^{\circ} \times 0.1^{\circ}$, a temporal coverage of January 1981 to the present, and data
133 formats of GRIB and NETCDF4.

134 To maintain consistency in the spatial and temporal resolutions of the fused data, we unified the ERA-Interim SWE data,
135 GLDAS SWE data, GlobSnow SWE data, AMSR-E/AMSR2 SWE data, and ERA5-land SWE data into a daily temporal
136 resolution, with a spatial resolution of 0.25° and geographic projection of the North Pole Lambert azimuthal equal area.

137 **2.3 Ridge regression machine learning algorithm for preparing the SWE**

138 In this study, we utilize the ridge regression model of a machine learning algorithm to fuse ERA-Interim SWE data (Dee et
139 al., 2011), GLDAS SWE data (Rodell et al., 2004), GlobSnow SWE data (Luoju et al., 2021), AMSR-E/AMSR2 SWE data
140 (Tedesco and Jeyaratnam, 2019), and ERA5-land SWE data (Muñoz Sabater, 2019) to generate a set of new RRM SWE
141 datasets. The target reference data in this study are the HSSC dataset and Russian snow survey data. The digital elevation

142 model (DEM) was used as an important environmental feature input to the ridge regression model and was included in the
 143 model training. The DEM is an auxiliary terrain feature variable in addition to the five SWE prediction feature variables,
 144 AMSR-E/AMSR2 SWE, ERA-Interim SWE, GLDAS SWE, GlobSnow SWE, and ERA5-land SWE.

145 The ridge regression model is a biased estimate regression method for collinear data analysis (Friedman et al., 2010; Hoerl
 146 and Kennard, 1970b, a). By abandoning the unbiasedness of the ordinary least squares, this algorithm can obtain the
 147 regression method in which the regression coefficient is more practical and reliable at the cost of losing part of the
 148 information and reducing the accuracy. The ridge regression model is flexible in the choice of predictor variables and does
 149 not require the predictor and target variables to be independent of each other. It can effectively solve the multicollinearity
 150 problem of predictor and target variables as well as reduce the impact of this problem on the training model (Duzan and
 151 Shariff, 2015; Saleh et al., 2019). Generally, reanalysis data based on SWE products cannot make the products and models
 152 independent of each other, i.e., they are prone to multicollinearity, which leads to distorted model estimation or difficulty in
 153 performing accurate estimations. In contrast, the ridge regression model can successfully solve the multicollinearity problem,
 154 i.e., the independence of training products and models. In addition, when integrating multiple SWE products, the accuracy of
 155 each SWE dataset is likely to differ. A small change in one of the SWE products involved in the training will cause a
 156 significant error in the final calculation results, while the ridge regression model has high accuracy and stability for these
 157 "ill-conditioned" SWE data. In addition, the main advantage of this model is that SWE products with long time series and
 158 large spatial scales are easy to prepare. The principle equation of the ridge regression model is defined as follows:

$$159 \quad \hat{\beta}^{ridge} = \underset{\beta}{\operatorname{argmin}} \left\{ \sum_{i=1}^N \left(y_i - \beta_0 - \sum_{j=1}^p x_{ij} \beta_j \right)^2 + \lambda \sum_{j=1}^p \beta_j^2 \right\}, \quad (1)$$

160 where $\hat{\beta}^{ridge}$ is the extremum solution function of ridge regression and p is the number of gridded SWE product variables
 161 involved in training. x_i are the prediction feature variables, which contain two parts: one set contains the main feature
 162 variables of the gridded SWE products, and the other part consists of the DEM auxiliary feature variables. y_i is the observed
 163 SWE, and λ , β , β_j and β_0 are the parameters to be solved. $1, \dots, N$ is the sample of the training dataset. $\lambda \sum_{j=1}^p \beta_j^2$ is the

164 penalty function term. The total number of samples N in the training dataset is 271651. The sample sizes of the training
165 dataset, validation dataset and test dataset are divided according to the ratio of 7:2:1, where the numbers of training set,
166 validation set and test set samples are 271651, 77614 and 38807, respectively. The model is developed in Python3, and the
167 model framework is based on the "scikit-learn" machine learning library (<https://scikit-learn.org/stable/index.html>). The code
168 is available upon request.

169 The integration process of the RRM SWE product (Fig. 2) is described as follows:

- 170 1) The original ERA-Interim SWE data, GLDAS SWE data, GlobSnow SWE data, AMSR-E/AMSR2 SWE data, ERA5-
171 land SWE data, DEM data, unified temporal resolution, spatial resolution, projection, spatial range, and unit are
172 preprocessed.
- 173 2) The spatiotemporal interpolation method is used to fill in the missing data of AMSR-E/AMSR2 SWE, ERA-Interim
174 SWE, and GlobSnow SWE in space and time. Based on this method, the missing AMSR-E/AMSR2 SWE data at low
175 latitudes and the missing ERA-Interim SWE and GlobSnow SWE data in the time series are added.
- 176 3) The SWE data observed at stations from 1979 to 2014 are used as sample training data, and the AMSR-E/AMSR2
177 SWE, ERA-Interim SWE, GLDAS SWE, GlobSnow SWE, ERA5-land SWE data, and DEM data are input into the
178 ridge regression model of a machine learning algorithm for training. During the RRM model training process, we
179 reconstructed the training data to try to extract training samples that are uniformly distributed spatially as much as
180 possible. First, a scan window of $250 \text{ km} \times 250 \text{ km}$ (10×10 pixels) was created. Then, each gridded SWE data point
181 participating in training is scanned, and the sample numbers in each scan window are counted. Finally, the mean value
182 n of the sample numbers in all scan windows is taken as the number of training samples to be selected in each scan
183 window. For the scan window with sample numbers higher than n , n samples are randomly selected from the scan
184 window. For the scan window with sample numbers lower than n , all samples in the scan window are selected as
185 training samples.
- 186 4) When the model was trained, ERA-Interim SWE, GLDAS SWE, GlobSnow SWE, and ERA5-land SWE were used as
187 the training data between 1979 and 2002 (AMSR-E/AMSR2 SWE data were not available before 2002), and AMSR-

188 E/AMSR2 SWE, ERA-Interim SWE, GLDAS SWE, GlobSnow SWE, and ERA5-land SWE were used as the training
189 data after 2002.

190 5) Based on the S-fold cross-validation method, the SWE data are continuously trained and validated, and the optimal
191 model and parameters are finally selected and evaluated by the loss function.

192 6) Based on the trained optimal model, multiple SWE data products are integrated into the time series, missing data are
193 predicted, and a set of spatiotemporally seamless SWE datasets is generated.

194 7) SWE data observed at stations from 2015 to 2018 are used to evaluate the accuracy of the RRM SWE product.

195 **2.4 Site data and evaluation metrics**

196 **2.4.1 Site SWE data for training, validation, and testing**

197 Russian snow survey data (<http://aisori.meteo.ru/ClimateR>) include the average snow depth data and the average snow
198 density data of the station, and the SWE is the product of the measured average snow depth and average snow density
199 (Bulygina et al., 2011). We obtained SWE data from 19493 stations from 1979-2016 from this dataset.

200 Hemispheric-scale snow course (hereafter referred to as HSSC) observational data are contained in a hemispheric-scale
201 SWE database based on SWE observational datasets from the former Soviet Union/Russia (FSU), Finland, and Canada
202 developed by Pulliainen et al. (Pulliainen et al., 2020; Bronnimann et al., 2018; Brown et al., 2019). This dataset is from the
203 website of the Finnish Meteorological Institute (FMI) (https://www.globsnow.info/swe/archive_v3.0/auxiliary_data/). The
204 dataset provides data from 2687 distributed regional snow course observations and contains 343,241 SWE observational data
205 points from 1979 to 2018. The snow courses of the HSSC dataset are transects in which SWE is sampled manually at
206 multiple locations with typical conditions to eliminate uncertainty in the regional-scale spatial variability of SWE due to the
207 influence of snowpack characteristics and land cover type (Pulliainen et al., 2020).

208 We carefully screened the Russian snow survey data and HSSC data and eliminated some abnormal observational data to
209 ensure the high quality of the training, validation, and test sets. The null and zero values are removed during the HSSC data
210 screening process. The null values, negative numbers, and extreme SWE values greater than 2000 mm are removed during
211 the Russian snow survey data screening process.

212 **2.4.2 Accuracy evaluation method for datasets**

213 Mean absolute error (MAE), root mean square error (RMSE), Pearson's correlation coefficient (R), and coefficient of
 214 determination (R^2) are used to evaluate the accuracies of AMSR-E/AMSR2 SWE, ERA-Interim SWE, GLDAS SWE,
 215 GlobSnow SWE, ERA5-land SWE, multisource data-averaged SWE, and the RRM SWE product. The specific equation of
 216 accuracy evaluation error is described as follows.

$$217 \quad MAE = \frac{1}{n} \sum_{i=1}^n |f_i - y_i|, \quad (2)$$

$$218 \quad RMSE = \left[\frac{\sum_{i=1}^n (f_i - y_i)^2}{n} \right]^{\frac{1}{2}}, \quad (3)$$

$$219 \quad R = \frac{1}{n-1} \sum_{i=1}^n \left(\frac{f_i - \bar{f}}{\sigma_f} \right) \left(\frac{y_i - \bar{y}}{\sigma_y} \right), \quad (4)$$

$$220 \quad R^2 = \frac{\sum_{i=1}^n (f_i - \bar{f})^2}{\sum_{i=1}^n (y_i - \bar{y})^2}, \quad (5)$$

221 where n is the number of samples in the validation dataset, f_i is the SWE dataset product, and y_i is the measured SWE at
 222 the station. \bar{f} and \bar{y} are the averages of SWE products and measured SWEs, respectively. σ_f and σ_y are the standard
 223 deviation of SWE products and measured SWEs, respectively.

224 To further evaluate the accuracy of the RRM SWE dataset at the spatial scale, we compared it with AMSR-E/AMSR2
 225 SWE, ERA-Interim SWE, GLDAS SWE, GlobSnow SWE, and ERA5-Land SWE at different altitude gradients. We also
 226 evaluated MAE, RMSE, R and R^2 separately for 11 elevation intervals: <100 m, 100-200 m, 200-300 m, 300-400 m, 400-
 227 500 m, 500-600 m, 600-700 m, 700-800 m, 800-900 m, 900-1000 m, and >1000 m. In addition, we evaluated the
 228 performances of the RRM SWE product in three representative regions: Russia, Canada, and Finland.

229 We used the Mann-Kendall trend test (Mann, 1945; Kendall, 1990) method to evaluate the variation trend in the RRM
230 SWE dataset from 1979 to 2019 and analyzed its reliability in terms of time series. Since the AMSR-E/AMSR2 SWE
231 product and the GlobSnow SWE product lack SWE data for Greenland, we removed the Greenland data to maintain
232 consistency in the spatial extent of the comparison data.

233 **3 Results and discussion**

234 **3.1 Overall accuracy evaluation of the RRM SWE product**

235 In this study, the accuracies of the RRM SWE, AMSR-E/AMSR2 SWE, ERA-Interim SWE, GLDAS SWE, GlobSnow
236 SWE, and ERA5-land SWE were compared using test datasets from 2015 to 2018. MAE, RMSE, R, and R^2 were used to
237 reflect the data quality of each SWE product. In addition, we compared the RRM SWE product with the SWE dataset
238 obtained by the multisource data average method.

239 According to the verification results in Fig. 3 and Table 2, the RRM SWE data have the best overall accuracy, and the
240 MAE, RMSE, R, and R^2 between the observed SWEs are 0.21, 25.37 mm, 0.89, and 0.79, respectively. The overall accuracy
241 of the GlobSnow SWE and ERA5-land SWE products is higher than that of other SWE products. The overall deviation of
242 the ERA5-land SWE products is the smallest except for the RRM SWE data, with MAE and RMSE values of 0.32 and 37.02
243 mm, respectively. The correlation between the ERA5-land SWE and observed SWE is the highest except for the RRM SWE
244 data, with R and R^2 values of 0.84 and 0.71, respectively. Although the overall deviation between the GlobSnow SWE
245 dataset and the measured SWE is small, its correlation with the measured value is low. The overall deviation between the
246 ERA5-land SWE dataset and the measured SWE is higher than that of the GlobSnow SWE dataset, but its estimation
247 accuracy for the high-value region of the SWE is low. In addition, the overall accuracy of the ERA-Interim SWE dataset and
248 GLDAS SWE dataset is relatively low, but their integrities are higher than those of the GlobSnow SWE dataset and AMSR-
249 E/AMSR2 SWE dataset in terms of temporal and spatial series. The AMSR-E/AMSR2 SWE dataset has a higher estimation
250 accuracy for the low-value SWE region. Moreover, in the land region above 45° N, most of the existing SWE data products
251 with regard to temporal and spatial degrees are missing to various degrees. Obviously, the accuracies of the existing SWE

252 products were uneven, as no type of SWE dataset is perfect.

253 The verification results also indicate the following ranking orders:

254 The MAE ranking order is RRM SWE < GlobSnow SWE = ERA5-land SWE < ERA-Interim SWE < multisource data
255 average SWE < AMSR-E/AMSR2 SWE < GLDAS SWE.

256 The RMSE ranking order is RRM SWE < ERA5-land SWE < GlobSnow SWE < ERA-Interim SWE < multisource data
257 average SWE < AMSR-E/AMSR2 SWE < GLDAS SWE.

258 The R ranking order is RRM SWE > ERA5-land SWE > GlobSnow SWE > ERA-Interim SWE > GLDAS SWE >
259 multisource data average SWE > AMSR-E/AMSR2 SWE.

260 The R² ranking order is RRM SWE > ERA5-land SWE > GlobSnow SWE > ERA-Interim SWE > GLDAS SWE >
261 multisource data average SWE > AMSR-E/AMSR2 SWE.

262 Compared with the ERA-Interim SWE, AMSR-E/AMSR2 SWE, GLDAS SWE, GlobSnow SWE, ERA5-land SWE, and
263 multisource data average SWE, the MAE of the RRM SWE and observed SWE is reduced by 0.22, 0.28, 0.37, 0.11, 0.11 and
264 0.23, respectively. The RMSE of the RRM SWE and observed SWE is reduced by 21.44 mm, 27.02 mm, 39.88 mm, 15.62
265 mm, 11.65 mm, and 26.63 mm, respectively. The correlation coefficients of the RRM SWE and observed SWE are improved
266 by 0.20, 0.42, 0.37, 0.19, 0.05, and 0.38, respectively. The coefficient of determination of the RRM SWE and observed SWE
267 is improved by 0.31, 0.57, 0.52, 0.30, 0.08, and 0.53, respectively. Although the multisource data average method can
268 improve the accuracy of SWE products to some extent (better than AMSR-E/AMSR2 SWE and GLDAS SWE), the
269 improvement of this method is still very limited. The RRM SWE product has a significant advantage over the multisource
270 data average method, and its accuracy is much higher than that of the simple multisource data average method (Table 2).
271 Based on the above verification results, the accuracy of the RRM SWE is significantly improved; the RRM SWE dataset has
272 higher accuracy than that of any single grid SWE dataset, and it also fills the gap in the original SWE data in terms of spatial
273 and temporal resolutions.

274 Based on the kernel density estimation method, we analyzed the density distribution of different SWE datasets (Fig. 4).
275 The results show that the RRM SWE dataset is closer to the 1:1 line and has the highest accuracy. The RRM SWE dataset is
276 particularly accurate for SWE estimation in the low-value region, and the test data are concentrated near the 1:1 line in the

277 high-density region (kernel density estimation > 0.00015) (Fig. 4). In contrast, the high-density regions of the GLDAS SWE
278 dataset, ERA-Interim SWE dataset, and AMSR-E/AMSR2 SWE dataset deviate significantly from the 1:1 line, resulting in
279 poor accuracy. The AMSR-E/AMSR2 SWE, GLDAS SWE, and GlobSnow SWE are underestimated relative to the SWE
280 measured at the site, among which GLDAS SWE underestimated the observed SWE the most seriously, while ERA5-land
281 SWE overestimated the observed SWE. Although the accuracies of GlobSnow SWE and ERA5-land SWE are relatively
282 high, their dispersion degrees are large (the kernel density estimation for most test data is less than 0.0001). Overall, the
283 RRM SWE data have a higher overall estimation accuracy, especially for the low-value area of SWE. For an SWE above
284 400 mm, the MAE and RMSE of the RRM SWE product and the measured SWE are 0.35 and 43.57 mm, respectively.
285 The estimation accuracy of the RRM SWE product for the high value range of SWE (SWE > 400 mm) is lower than that for
286 the low value range of SWE (SWE < 400 mm) (Fig. 4). The main reason for this is that the training accuracy of the RRM
287 model for the high-value range of SWE is affected by the small number of stations that observe the high-value range of
288 SWE.

289 However, in this study, there are still some uncertainties in the ridge regression machine learning algorithm that integrates
290 SWE products. First, this model is strongly dependent on on-site observational data, and the fusion precision of SWE is poor
291 in some areas with sparse observational stations. The fusion accuracy of SWE products will be affected to a certain extent
292 without considering the prior snow cover information. The RRM SWE product is still underestimated in cases of high SWE.
293 Then, in addition to the DEM, meteorological elements, NDVI, land type, and other factors will affect the SWE estimation.
294 Unfortunately, our current RRM presented here does not consider these factors as predictors, which is a limitation of the
295 current RRM SWE product. Finally, in complex terrain with an elevation interval >1000 m, the RRM SWE product
296 performed poorly, with an RMSE of 31.14 mm (Fig. 5), and the integration of SWE products remains challenging (Mortimer
297 et al., 2020).

298 **3.2 Accuracy evaluation of the RRM SWE product at different altitudes and regions**

299 The accuracy of each SWE product is not absolute at different altitude gradients based on evaluations of the AMSR-
300 E/AMSR2 SWE, ERA-Interim SWE, GLDAS SWE, GlobSnow SWE, and ERA5-land SWE product accuracies (Fig. 5).

301 The accuracy of a single SWE product is different from its overall accuracy. We consider the influence of altitude in the
302 algorithm and make full use of the accuracy advantage of each SWE data for different altitude gradients.

303 The above verification results show that the MAE, RMSE, R and R^2 between the RRM SWE product and measured SWE
304 perform well at altitude gradients of <100 m, 100-200 m, 200-300 m, 300-400 m, 400-500 m, 500-600 m, 600-700 m, 700-
305 800 m, 800-900 m, 900-1000 m and >1000 m (Fig. 5). Overall, the RRM SWE product has the highest accuracy in the
306 elevation intervals of <100 m, 100-200 m, 200-300 m, 400-500 m, 500-600 m, 600-700 m, 700-800 m, 800-900 m,
307 and >1000 m. The RRM SWE product itself has the best performance in the elevation interval <100 m. The ERA5-land
308 product has the best performance in the elevation interval 300-400 m. The GlobSnow product has the best performance in
309 the elevation interval 900-1000 m.

310 The RRM SWE product has good performance in different regions, and its RMSE in Russia, Canada, and Finland are
311 26.39 mm, 29.31 mm, and 25.29 mm, respectively; additionally, the performance of the RRM SWE product in different
312 regions is basically similar (Table 3). The RRM SWE product performs well not only at different altitudes but also in
313 different regions, and it has good stability.

314 **3.3 Comparison of spatial distribution patterns between the RRM SWE product and traditional SWE products**

315 A comparison of the spatially distributed annual average SWE distributions is made between the RRM SWE and AMSR-
316 E/AMSR2 SWE, ERA-Interim SWE, GLDAS SWE, GlobSnow SWE, and ERA5-land SWE in 2014, 2015, 2016, and 2017,
317 and their spatial distribution patterns are shown in Fig. 6.

318 Overall, the RRM SWE dataset, AMSR-E/AMSR2 SWE dataset, ERA-Interim SWE dataset, GLDAS SWE dataset,
319 GlobSnow SWE dataset, and ERA5-land SWE dataset have similar spatial distribution patterns in the land region above 45°
320 N, showing a trend of lower SWE in low latitudes and higher SWE in high latitudes. The AMSR-E/AMSR2 SWE dataset
321 covers a limited extent in the land region above 45° N, many data points are missing, and low SWE values exist at low
322 latitudes. In northern Siberia, the ERA-Interim SWE product has a higher SWE, and there are many abnormal, extreme SWE
323 values (SWE > 500 mm) in this dataset. In low-latitude regions, such as Alaska, North Siberia, and the easternmost region of
324 Russia, the SWE of GLDAS SWE products is significantly lower. The GlobSnow SWE product lacks SWE data for

325 Greenland, and this dataset has low SWEs in the Baffin Island, Koryak Mountains, Kamchatka Peninsula, and Alaska
326 regions. The ERA5-land SWE products have low SWEs in northeastern Russia, Scandinavia, and northeastern Canada. The
327 RRM SWE dataset is more reasonable for estimating the spatial distribution of SWE in the land region above 45° N, and the
328 data integrity is higher. Moreover, based on the new machine learning algorithm, a variety of SWE data products in different
329 time series are fused, which makes the RRM SWE dataset completely temporally and spatially continuous.

330 The relative difference between the RRM SWE data and GLDAS SWE data is the highest, and the relative difference is
331 greater than 80% in most low altitude regions (Fig. 7). The relative difference between the RRM SWE data and the
332 GlobSnow SWE data is relatively small overall, especially in most high-latitude areas where the relative difference is less
333 than 10% (Fig. 7). Overall, the annual average relative differences in the RRM SWE data and AMSR2 SWE, ERA-Interim
334 SWE, GLDAS SWE, GlobSnow SWE, and ERA5-land SWE are 37%, 41%, 54%, 25%, and 29%, respectively (Fig. 7).
335 Previous studies have shown that the accuracy of the SWE in the Northern Hemisphere estimated by GlobSnow SWE data is
336 higher (Pulliainen et al., 2020), while the spatial distribution pattern of the RRM SWE data is close to the estimation result of
337 GlobSnow SWE. In addition, the single point verification results based on the measured SWE data of meteorological stations
338 in section 3.1 show that the RRM SWE dataset has higher accuracy than the GlobSnow SWE dataset. The RRM SWE
339 dataset has good accuracy.

340 **3.4 Comparison of the annual variation tendencies of AMSR-E/AMSR2 SWE, ERA-Interim SWE, GLDAS SWE,** 341 **GlobSnow SWE, and ERA5-land SWE and the RRM SWE in the land region above 45° N**

342 Based on the Mann-Kendall trend test, we analyzed the changing trend in the region-wide annual average SWE of the
343 AMSR-E/AMSR2 SWE, ERA-Interim SWE, GLDAS SWE, GlobSnow SWE, ERA5-land SWE, and RRM SWE in the land
344 region above 45° N from 1979 to 2019.

345 Based on the Mann-Kendall trend test (see Fig. 8 and Table 4), from 1979 to 2019, the test value of the ERA-Interim
346 region-wide annual average SWE is 1.08, and there is no significant change trend under the significance test level of 0.05.
347 The test value of the GLDAS region-wide annual average SWE was 4.95 and showed a significant increasing trend at the
348 significance test level of 0.05. The test values of the AMSR-E/AMSR2 annual average SWE, GlobSnow annual average

349 SWE, ERA5-land annual average SWE, and RRM annual average SWE are -3.26, -2.54, -3.43, and -3.00, respectively, and
350 these four SWEs showed a significant decreasing trend at the significance test level of 0.05. Based on the analysis of the
351 RRM SWE product, between 1979 and 2019, the region-wide annual average SWE in the land region above 45° N decreased
352 by 15.1 percent. In the Northern Hemisphere, spring snow cover extent has decreased significantly, according to the Fifth
353 Assessment Report (AR5) of the IPCC. Between 1967 and 2010, the spring snow cover extent decreased by an average of
354 1.6 percent per decade, while the June snow cover extent decreased by 11.7 percent per decade (Stocker, 2014). Most studies
355 have shown that the annual variation tendency of snow depth and snow cover extent showed a significant decreasing trend in
356 the Northern Hemisphere (Brutel-Vuilmet et al., 2013), which is consistent with the annual variation tendency of the RRM
357 SWE dataset. This dataset can reflect the characteristics of snow cover change in the land region above 45° N in light of
358 climate change and can be used as the driving data for climate models to support climate change-related research. In
359 addition, this dataset is expected to provide a snow data basis for the study of "Arctic amplification".

360 **4 Data availability**

361 The RRM SWE product is available for free download from ‘A Big Earth Data Platform for Three Poles’
362 (<http://dx.doi.org/10.11888/Snow.tpd.271556>) (Li et al., 2021). The temporal resolution of the RRM SWE product is daily,
363 and the spatial resolution is 10 km. It spans latitudes of 45°N-90°N and longitudes of 180°W-180°E. A brief summary and
364 data description document (including data details, spatial range, and usage method) are also provided.

365 **5 Conclusions**

366 In this study, we propose a method to fuse multisource SWE data by a ridge regression model based on machine learning. A
367 new method was utilized to prepare a set of spatiotemporally seamless SWE datasets of the RRM SWE, combined with the
368 original AMSR-E/AMSR2 SWE, ERA-Interim SWE, GLDAS SWE, GlobSnow SWE, and ERA5-land SWE datasets. In the
369 RRM SWE dataset, the time series of the data is 1979-2019, the temporal resolution is daily, the spatial resolution is 10 km,
370 and the spatial range is the land region above 45° N.

371 The RRM SWE data product has the best accuracy, especially for the estimation of low SWE. The accuracy ranking of the
372 SWE dataset verified by the test dataset is described as follows: RRM SWE > ERA5-land SWE > GlobSnow SWE > ERA-
373 Interim SWE > multisource data average SWE > AMSR-E/AMSR2 SWE > GLDAS SWE. The accuracy of the RRM SWE
374 dataset is higher than that of the existing SWE products at most elevation intervals. The RRM SWE product has good
375 performance and stability in different regions. Moreover, the RRM SWE dataset spatiotemporally fills in the missing data of
376 the original SWE dataset.

377 Compared with traditional fusion methods, machine learning methods have a strong advantage. We find that the simple
378 machine learning algorithm has not only high efficiency but also good accuracy in the preparation of SWE products on a
379 global scale. Without losing the advantages of existing SWE products, this method can also make full use of station
380 observational data to integrate the advantages of various SWE products. The model training process does not rely too much
381 on a specific sample, and this model has a strong generalization ability. In addition, the influence of altitude on the
382 preparation scheme is considered in detail in the model. Compared with the SWE dataset prepared by the traditional method,
383 the spatial resolution is only 25 km, while this new method obtains an SWE dataset with a higher spatial resolution of 10 km.

384 We propose that the RRM SWE dataset preparation scheme has good continuity and can prepare real-time and high-
385 quality SWE datasets in the land region above 45° N. In addition, the new method proposed in this paper has the advantages
386 of simplicity and high precision in preparing large-scale SWE datasets and can be easily extended to the preparation of other
387 snow datasets. This dataset is an important supplement to the land region above the 45° N SWE database and is expected to
388 provide data support for Arctic cryosphere studies and global climate change studies.

389 **Author contributions.**

390 DS and HL designed the study and wrote the manuscript; JW, XH, and TC contributed to the discussions, edits, and
391 revisions. DS and WJ compiled the model code.

392 **Competing interests.**

393 The authors declare that they have no conflicts of interest.

394 **Acknowledgments.**

395 The authors would like to thank the European Space Agency (ESA) for providing the GlobSnow data, the European Centre
396 for Medium-Range Weather Forecasts (ECMWF) for ERA-Interim data and ERA5-land data, the National Aeronautics and
397 Space Administration (NASA) for the AMSR-E/AMSR2 data, the Goddard Earth Sciences Data and Information Services
398 Center (GESDISC) for the GLDAS data, the Russian Federal Service for Hydrometeorology and Environmental Monitoring
399 (ROSHYDROMET) for the snow survey data, and the Finnish Meteorological Institute (FMI) for the hemispheric-scale
400 snow course (HSSC) observational data.

401 **Financial support.**

402 This research was supported by the Strategic Priority Research Program of the Chinese Academy of Sciences (Grant No.
403 XDA19070302), the National Science Fund for Distinguished Young Scholars (Grant No. 42125604), and the National
404 Natural Science Foundation of China (Grant No. 41971399, 41971325, 42171391).

405 **References**

406 Bair, E. H., Abreu Calfa, A., Rittger, K., and Dozier, J.: Using machine learning for real-time estimates of snow water
407 equivalent in the watersheds of Afghanistan, *The Cryosphere*, 12, 1579-1594, 2018.

408 Balsamo, G., Albergel, C., Beljaars, A., Boussetta, S., Brun, E., Cloke, H., Dee, D., Dutra, E., Munoz-Sabater, J.,
409 Pappenberger, F., de Rosnay, P., Stockdale, T., and Vitart, F.: ERA-Interim/Land: a global land surface reanalysis data set,
410 *Hydrol Earth Syst Sc*, 19, 389-407, 10.5194/hess-19-389-2015, 2015.

411 Barnett, T. P., Adam, J. C., and Lettenmaier, D. P.: Potential impacts of a warming climate on water availability in snow-
412 dominated regions, *Nature*, 438, 303-309, 10.1038/nature04141, 2005.

413 Bintanja, R. and Andry, O.: Towards a rain-dominated Arctic, *Nat Clim Change*, 7, 263+, 10.1038/Nclimate3240, 2017.

414 Bronnimann, S., Allan, R., Atkinson, C., Buizza, R., Bulygina, O., Dahlgren, P., Dee, D., Dunn, R., Gomes, P., John, V. O.,
415 Jourdain, S., Haimberger, L., Hersbach, H., Kennedy, J., Poli, P., Pulliainen, J., Rayner, N., Saunders, R., Schulz, J., Sterin,
416 A., Stickler, A., Titchner, H., Valente, M. A., Ventura, C., and Wilkinson, C.: Observations for Reanalyses, *Bulletin of the*
417 *American Meteorological Society*, 99, 1851-1866, 10.1175/Bams-D-17-0229.1, 2018.

418 Brown, R. D., Fang, B., and Mudryk, L.: Update of Canadian historical snow survey data and analysis of snow water
419 equivalent trends, 1967–2016, *Atmosphere-Ocean*, 57, 149-156, 2019.

420 Broxton, P. D., Van Leeuwen, W. J., and Biederman, J. A.: Improving snow water equivalent maps with machine learning of
421 snow survey and lidar measurements, *Water Resources Research*, 55, 3739-3757, 2019.

422 Brutel-Vuilmet, C., Menegoz, M., and Krinner, G.: An analysis of present and future seasonal Northern Hemisphere land
423 snow cover simulated by CMIP5 coupled climate models, *Cryosphere*, 7, 67-80, 10.5194/tc-7-67-2013, 2013.

424 Bulygina, O. N., Groisman, P. Y., Razuvaev, V. N., and Korshunova, N. N.: Changes in snow cover characteristics over
425 Northern Eurasia since 1966, *Environmental Research Letters*, 6, Artn 04520410.1088/1748-9326/6/4/045204, 2011.

426 Dee, D. P., Uppala, S. M., Simmons, A., Berrisford, P., Poli, P., Kobayashi, S., Andrae, U., Balmaseda, M., Balsamo, G., and
427 Bauer, d. P.: The ERA - Interim reanalysis: Configuration and performance of the data assimilation system, *Quarterly*
428 *Journal of the royal meteorological society*, 137, 553-597, 2011.

429 Duzan, H. and Shariff, N. S. B. M.: Ridge regression for solving the multicollinearity problem: review of methods and
430 models, *Journal of Applied Science*, 2015.

431 Friedman, J., Hastie, T., and Tibshirani, R.: Regularization Paths for Generalized Linear Models via Coordinate Descent, *J*
432 *Stat Softw*, 33, 1-22, DOI 10.18637/jss.v033.i01, 2010.

433 Gelaro, R., McCarty, W., Suarez, M. J., Todling, R., Molod, A., Takacs, L., Randles, C. A., Darmenov, A., Bosilovich, M. G.,
434 Reichle, R., Wargan, K., Coy, L., Cullather, R., Draper, C., Akella, S., Buchard, V., Conaty, A., da Silva, A. M., Gu, W., Kim,
435 G. K., Koster, R., Lucchesi, R., Merkova, D., Nielsen, J. E., Partyka, G., Pawson, S., Putman, W., Rienecker, M., Schubert,
436 S. D., Sienkiewicz, M., and Zhao, B.: The Modern-Era Retrospective Analysis for Research and Applications, Version 2
437 (MERRA-2), *J Climate*, 30, 5419-5454, 10.1175/Jcli-D-16-0758.1, 2017.

438 Guilkey, D. K. and Murphy, J. L.: Directed Ridge Regression Techniques in Cases of Multicollinearity, *J Am Stat Assoc*, 70,
439 769-775, 1975.

440 Henderson, G. R., Peings, Y., Furtado, J. C., and Kushner, P. J.: Snow-atmosphere coupling in the Northern Hemisphere, *Nat*
441 *Clim Change*, 8, 954-+, 10.1038/s41558-018-0295-6, 2018.

442 Hoerl, A. E. and Kennard, R. W.: Ridge regression: applications to nonorthogonal problems, *Technometrics*, 12, 69-82,
443 1970a.

444 Hoerl, A. E. and Kennard, R. W.: Ridge regression: Biased estimation for nonorthogonal problems, *Technometrics*, 12, 55-
445 67, 1970b.

446 Imaoka, K., Kachi, M., Fujii, H., Murakami, H., Hori, M., Ono, A., Igarashi, T., Nakagawa, K., Oki, T., Honda, Y., and
447 Shimoda, H.: Global Change Observation Mission (GCOM) for Monitoring Carbon, Water Cycles, and Climate Change, *P*
448 *Ieee*, 98, 717-734, 10.1109/Jproc.2009.2036869, 2010.

449 IPCC, 2021: Climate Change 2021: The Physical Science Basis. Contribution of Working Group I to the Sixth Assessment
450 Report of the Intergovernmental Panel on Climate Change [Masson-Delmotte, V., P. Zhai, A. Pirani, S.L. Connors, C. Péan,
451 S. Berger, N. Caud, Y. Chen, L. Goldfarb, M.I. Gomis, M. Huang, K. Leitzell, E. Lonnoy, J.B.R. Matthews, T.K. Maycock,
452 T. Waterfield, O. Yelekçi, R. Yu, and B. Zhou (eds.)]. Cambridge University Press. In Press.

453 Kelly, R.: The AMSR-E Snow Depth Algorithm: Description and Initial Results, 2009.

454 Kendall, M. G.: Rank Correlation Methods, *British Journal of Psychology*, 25, 86–91, 1990.

455 Li, H., Shao, D., Li, H., Wang, W., Ma, Y., and Lei, H.: Arctic Snow Water Equivalent Grid Dataset (1979-2019), A Big
456 Earth Data Platform for Three Poles [dataset], 10.11888/Snow.tpd.271556, 2021.

457 Luoju, K., Pulliainen, J., Takala, M., Lemmetyinen, J., Mortimer, C., Derksen, C., Mudryk, L., Moisander, M., Hiltunen,
458 M., and Smolander, T.: GlobSnow v3. 0 Northern Hemisphere snow water equivalent dataset, *Scientific Data*, 8, 1-16, 2021.

459 Mann, H. B.: Nonparametric test against trend, *Econometrica*, 13, 245-259, 1945.

460 Menne, M., Durre, I., Korzeniewski, B., McNeal, S., Thomas, K., Yin, X., Anthony, S., Ray, R., Vose, R., and Gleason, B.:
461 Global Historical Climatology Network–Daily (GHCN-Daily), Version, 3, V5D21VHZ, 2016.

462 Mortimer, C., Mudryk, L., Derksen, C., Luoju, K., Brown, R., Kelly, R., and Tedesco, M.: Evaluation of long-term Northern

463 Hemisphere snow water equivalent products, *The Cryosphere*, 14, 1579-1594, 2020.

464 Mudryk, L., Derksen, C., Kushner, P., and Brown, R.: Characterization of Northern Hemisphere snow water equivalent
465 datasets, 1981–2010, *Journal of Climate*, 28, 8037-8051, 2015a.

466 Mudryk, L. R., Derksen, C., Kushner, P. J., and Brown, R.: Characterization of Northern Hemisphere Snow Water Equivalent
467 Datasets, 1981-2010, *J Climate*, 28, 8037-8051, 10.1175/Jcli-D-15-0229.1, 2015b.

468 Muñoz Sabater, J.: ERA5-Land hourly data from 1981 to present, Copernicus Climate Change Service (C3S) Climate Data
469 Store (CDS), 2019.

470 Ntokas, K. F., Odry, J., Boucher, M.-A., and Garnaud, C.: Investigating ANN architectures and training to estimate snow
471 water equivalent from snow depth, *Hydrology and Earth System Sciences*, 25, 3017-3040, 2021.

472 Pan, M., Fisher, C. K., Chaney, N. W., Zhan, W., Crow, W. T., Aires, F., Entekhabi, D., and Wood, E. F.: Triple collocation:
473 Beyond three estimates and separation of structural/non-structural errors, *Remote Sens Environ*, 171, 299-310,
474 10.1016/j.rse.2015.10.028, 2015.

475 Pan, M., Sheffield, J., Wood, E. F., Mitchell, K. E., Houser, P. R., Schaake, J. C., Robock, A., Lohmann, D., Cosgrove, B.,
476 and Duan, Q.: Snow process modeling in the North American Land Data Assimilation System (NLDAS): 2. Evaluation of
477 model simulated snow water equivalent, *Journal of Geophysical Research: Atmospheres*, 108, 2003.

478 Pulliainen, J.: Mapping of snow water equivalent and snow depth in boreal and sub-arctic zones by assimilating space-borne
479 microwave radiometer data and ground-based observations, *Remote Sens Environ*, 101, 257-269, 10.1016/j.rse.2006.01.002,
480 2006.

481 Pulliainen, J., Luojus, K., Derksen, C., Mudryk, L., Lemmetyinen, J., Salminen, M., Ikonen, J., Takala, M., Cohen, J.,
482 Smolander, T., and Norberg, J.: Patterns and trends of Northern Hemisphere snow mass from 1980 to 2018 (vol 41, pg 861,
483 2020), *Nature*, 582, E18-E18, 10.1038/s41586-020-2416-4, 2020.

484 Reichle, R. H., Koster, R. D., De Lannoy, G. J. M., Forman, B. A., Liu, Q., Mahanama, S. P. P., and Toure, A.: Assessment
485 and Enhancement of MERRA Land Surface Hydrology Estimates, *J Climate*, 24, 6322-6338, 10.1175/Jcli-D-10-05033.1,
486 2011.

487 Rodell, M., Houser, P., Jambor, U., Gottschalck, J., Mitchell, K., Meng, C.-J., Arsenault, K., Cosgrove, B., Radakovich, J.,

488 and Bosilovich, M.: The global land data assimilation system, *Bulletin of the American Meteorological Society*, 85, 381-394,
489 2004.

490 Saleh, A. M. E., Arashi, M., and Kibria, B. G.: Theory of ridge regression estimation with applications, John Wiley &
491 Sons2019.

492 Santi, E., Brogioni, M., Leduc-Leballeur, M., Macelloni, G., Montomoli, F., Pampaloni, P., Lemmetyinen, J., Cohen, J., Rott,
493 H., and Nagler, T.: Exploiting the ANN Potential in Estimating Snow Depth and Snow Water Equivalent From the Airborne
494 SnowSAR Data at X-and Ku-Bands, *IEEE Transactions on Geoscience and Remote Sensing*, 2021.

495 Snauffer, A. M., Hsieh, W. W., and Cannon, A. J.: Comparison of gridded snow water equivalent products with in situ
496 measurements in British Columbia, Canada, *J Hydrol*, 541, 714-726, 10.1016/j.jhydrol.2016.07.027, 2016.

497 Snauffer, A. M., Hsieh, W. W., Cannon, A. J., and Schnorbus, M. A.: Improving gridded snow water equivalent products in
498 British Columbia, Canada: multi-source data fusion by neural network models, *Cryosphere*, 12, 891-905, 10.5194/tc-12-891-
499 2018, 2018.

500 Stocker, T.: Climate change 2013: the physical science basis: Working Group I contribution to the Fifth assessment report of
501 the Intergovernmental Panel on Climate Change, Cambridge university press2014.

502 Tedesco, M. and Jeyaratnam, J.: AMSR-E/AMSR2 Unified L3 Global Daily 25 km EASE-Grid Snow Water Equivalent,
503 Version 1.[online] Boulder, Colorado USA, NASA National Snow and Ice Data Center Distributed Active Archive Center,
504 2019.

505 Vuyovich, C. M., Jacobs, J. M., and Daly, S. F.: Comparison of passive microwave and modeled estimates of total watershed
506 SWE in the continental U nited S tates, *Water resources research*, 50, 9088-9102, 2014.

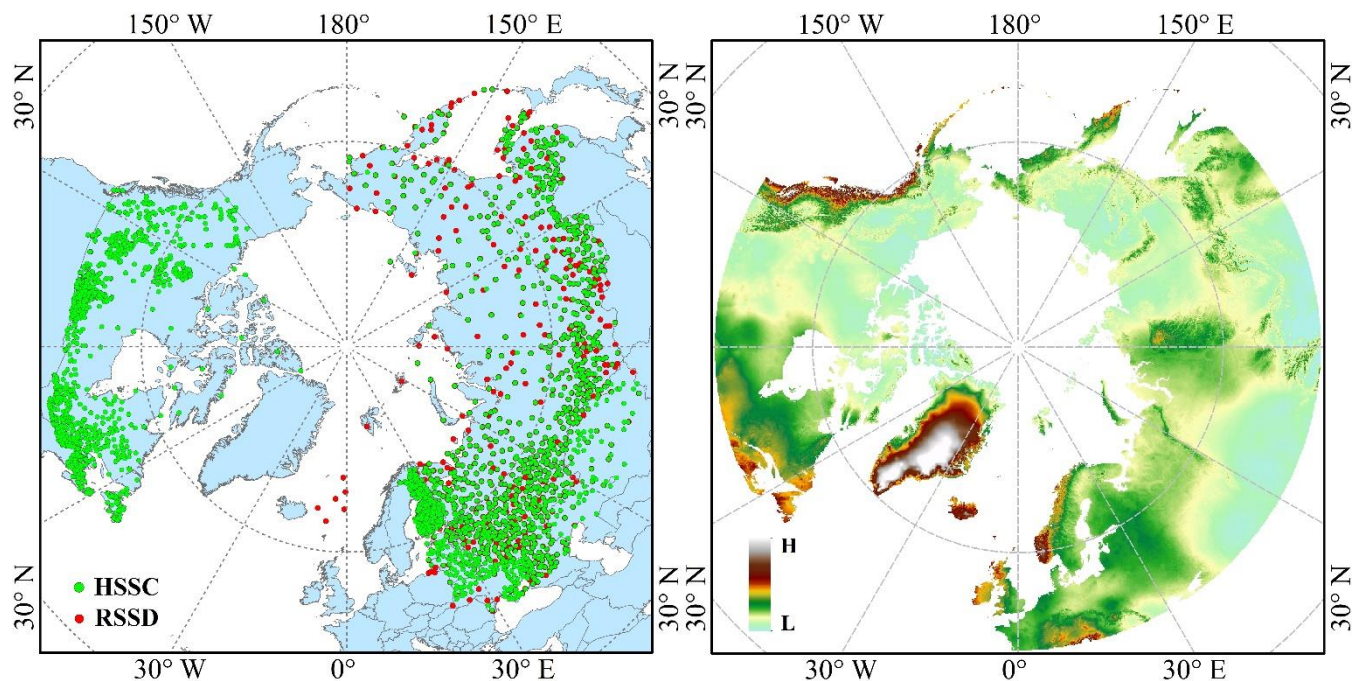
507 Walker, A., Brasnett, B., and Brown, R.: Canadian Meteorological Centre (CMC) daily gridded snow depth analysis for
508 Northern Hemisphere, 1998-2008, 2011.

509 Wang, J. W., Yuan, Q. Q., Shen, H. F., Liu, T. T., Li, T. W., Yue, L. W., Shi, X. G., and Zhang, L. P.: Estimating snow depth
510 by combining satellite data and ground-based observations over Alaska: A deep learning approach, *J Hydrol*, 585, ARTN
511 12482810.1016/j.jhydrol.2020.124828, 2020.

512 Xiao, X. X., Zhang, T. J., Zhong, X. Y., Shao, W. W., and Li, X. D.: Support vector regression snow-depth retrieval algorithm

513 using passive microwave remote sensing data, Remote Sens Environ, 210, 48-64, 10.1016/j.rse.2018.03.008, 2018.

514



515

516 **Figure 1: The DEM and snow survey stations of the research region. The right subgraph shows the DEM, and the left subgraph**

517 **shows the SWE observational stations. HSSC, hemispheric-scale snow course; RSSD, the Russian snow survey station. The spatial**

518 **range of the RRM SWE product is consistent with that of the DEM.**

519

520

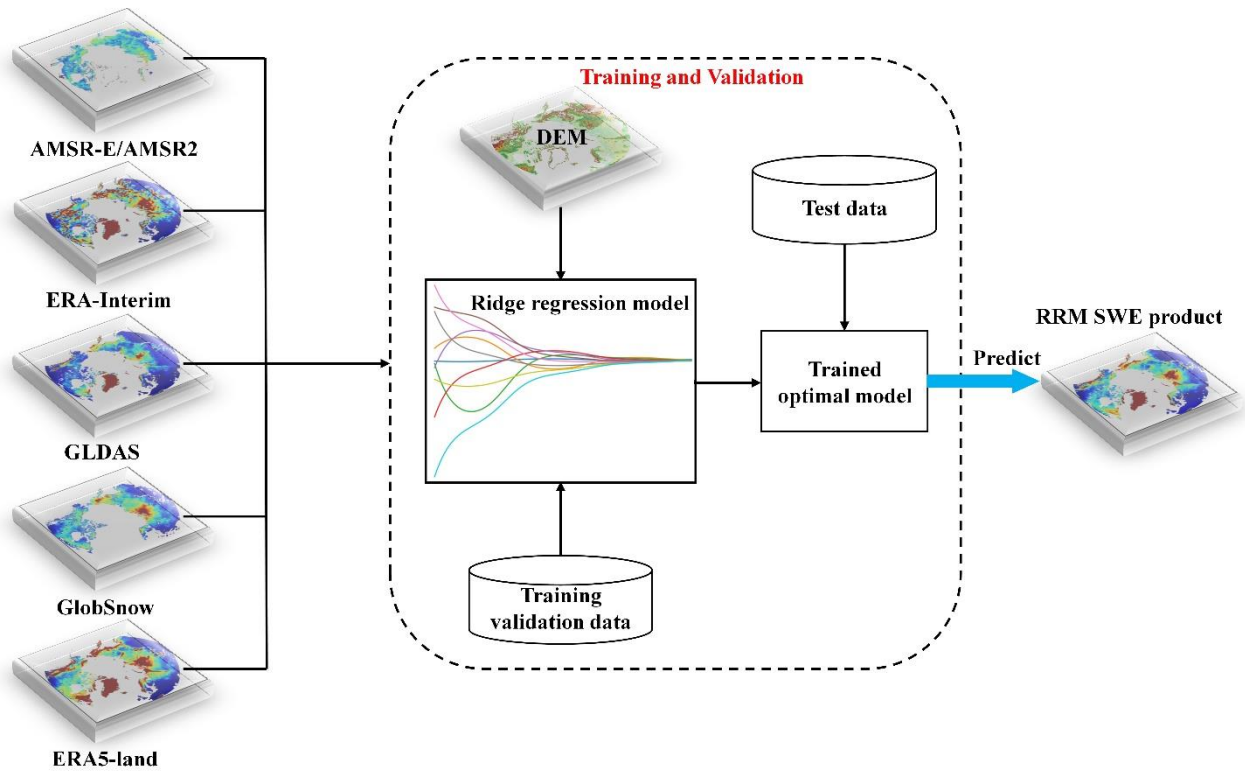
Table 1: Introduction to the SWE data.

Data type	Data name	Time series	Temporal resolution	Spatial resolution	Spatial coverage	File format
Remote sensing data	AMSR-E/AMSR2	2002-2011/2012-2020	Daily	25 km x 25 km	Global (No Greenland)	HDF5
Data assimilation dataset	GLDAS	1979-2020	Daily	0.25°×0.25°	Global	NetCDF
	GlobSnow	1979-2018	Daily	0.25°×0.25°	Northern Hemisphere (No Greenland)	NetCDF
Reanalysis dataset	ERA-Interim	1979-2019	Daily	0.25°×0.25°	Global	NetCDF
	ERA5-land	1981- present	Hour	0.1°×0.1°	Global	NetCDF

522

523

524



525

526

Figure 2: Flow chart of the RRM SWE data preparation (preparation of spatiotemporal seamless SWE datasets mainly includes

527

three processes: model training, model reasoning, and SWE data preparation).

528

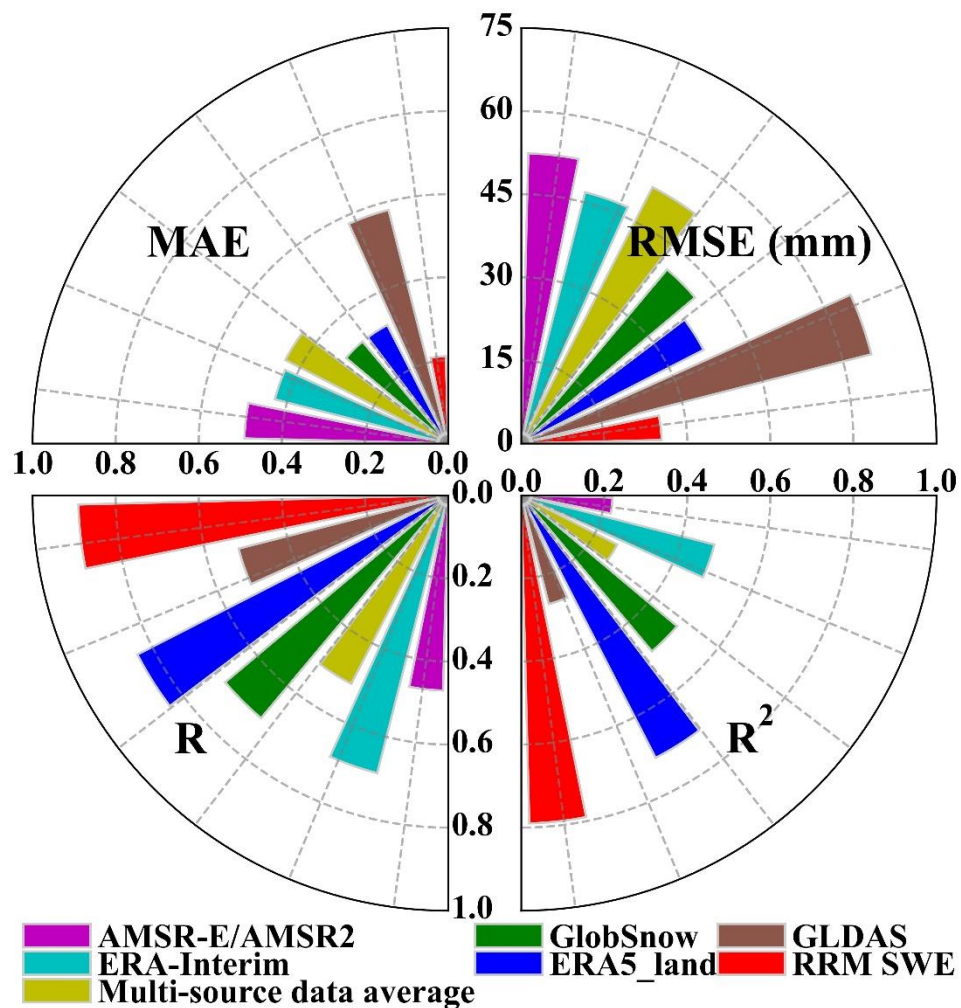
529

530 **Table 2: Error list for the station data and grid snow water equivalent products.**

Error type	MAE	RMSE (mm)	R	R²
ERA-Interim	0.43	46.81	0.69	0.48
AMSR-E/AMSR2	0.49	52.39	0.47	0.22
GLDAS	0.58	65.25	0.52	0.27
GlobSnow	0.32	40.99	0.70	0.49
ERA5-land	0.32	37.02	0.84	0.71
Multisource data average	0.44	52.00	0.51	0.26
RRM SWE	0.21	25.37	0.89	0.79

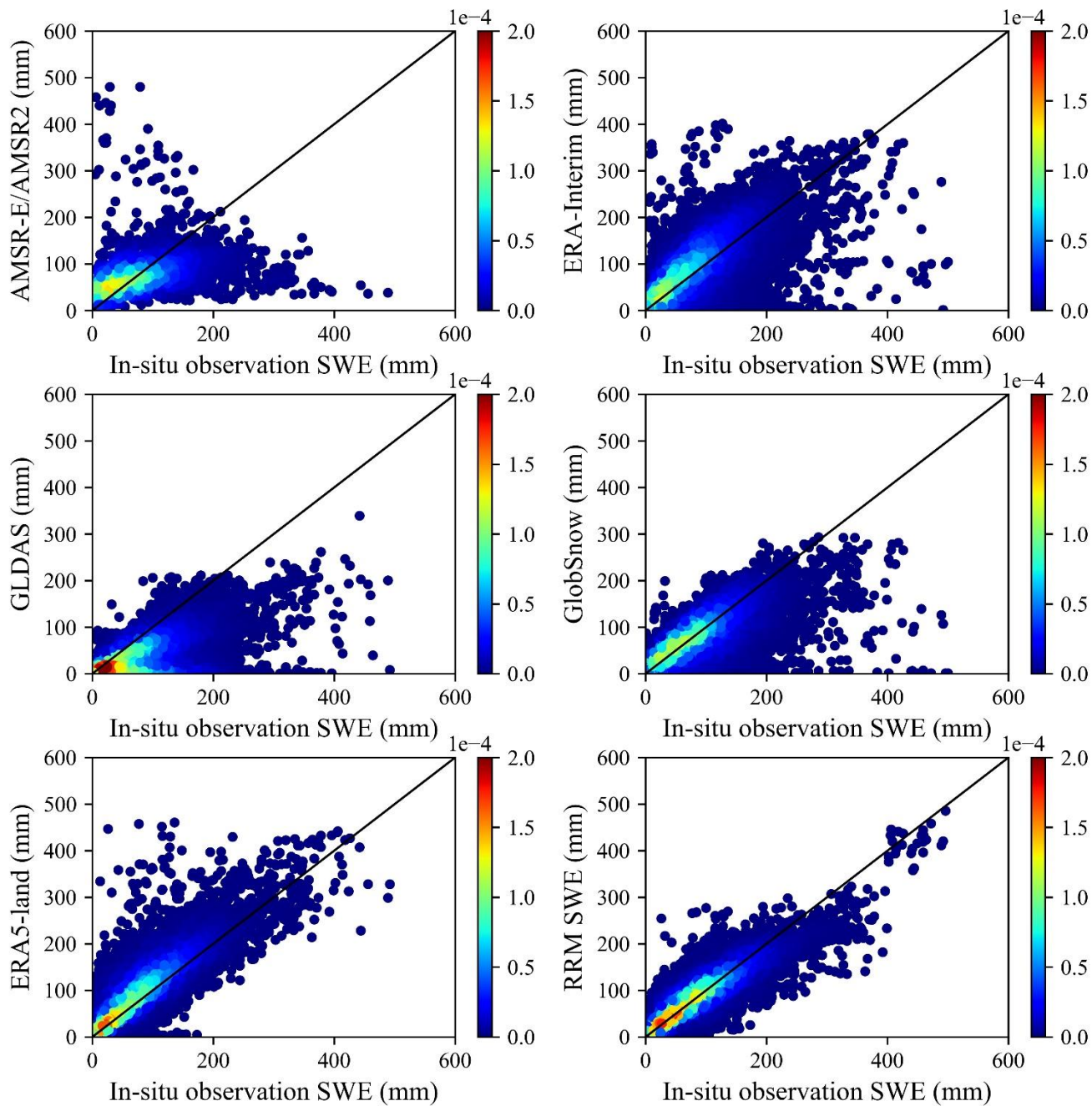
531

532



533

534 **Figure 3: Accuracy comparison of various SWE products.** The upper left sector represents the MAE, the upper right sector
 535 represents the RMSE, the lower left sector represents R, and the lower right sector represents R². The sector axis represents the
 536 size of the error, and the color represents different SWE datasets.



537

538

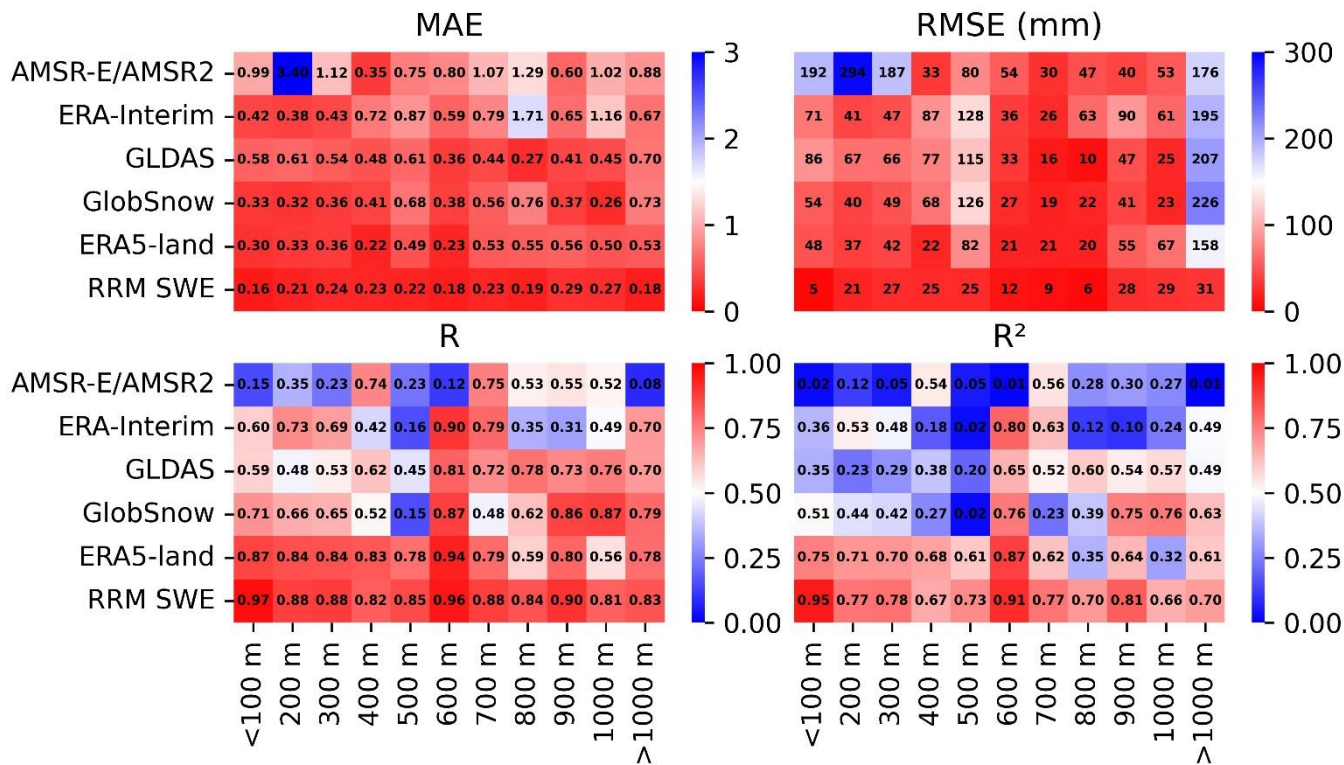
Figure 4: Error verification density diagram (a total of 38807 sample points were used for verification). The color bar represents

539

the value of kernel density estimation. The closer the high-density area is to the 1:1 line, the higher the verification accuracy of the

540

dataset is at most of the measuring stations.



541

542

543

544

545

546

547

548

549

550

551

552

553

554

555

556

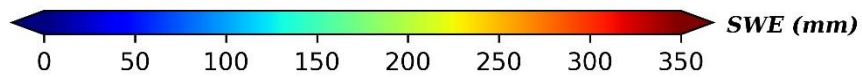
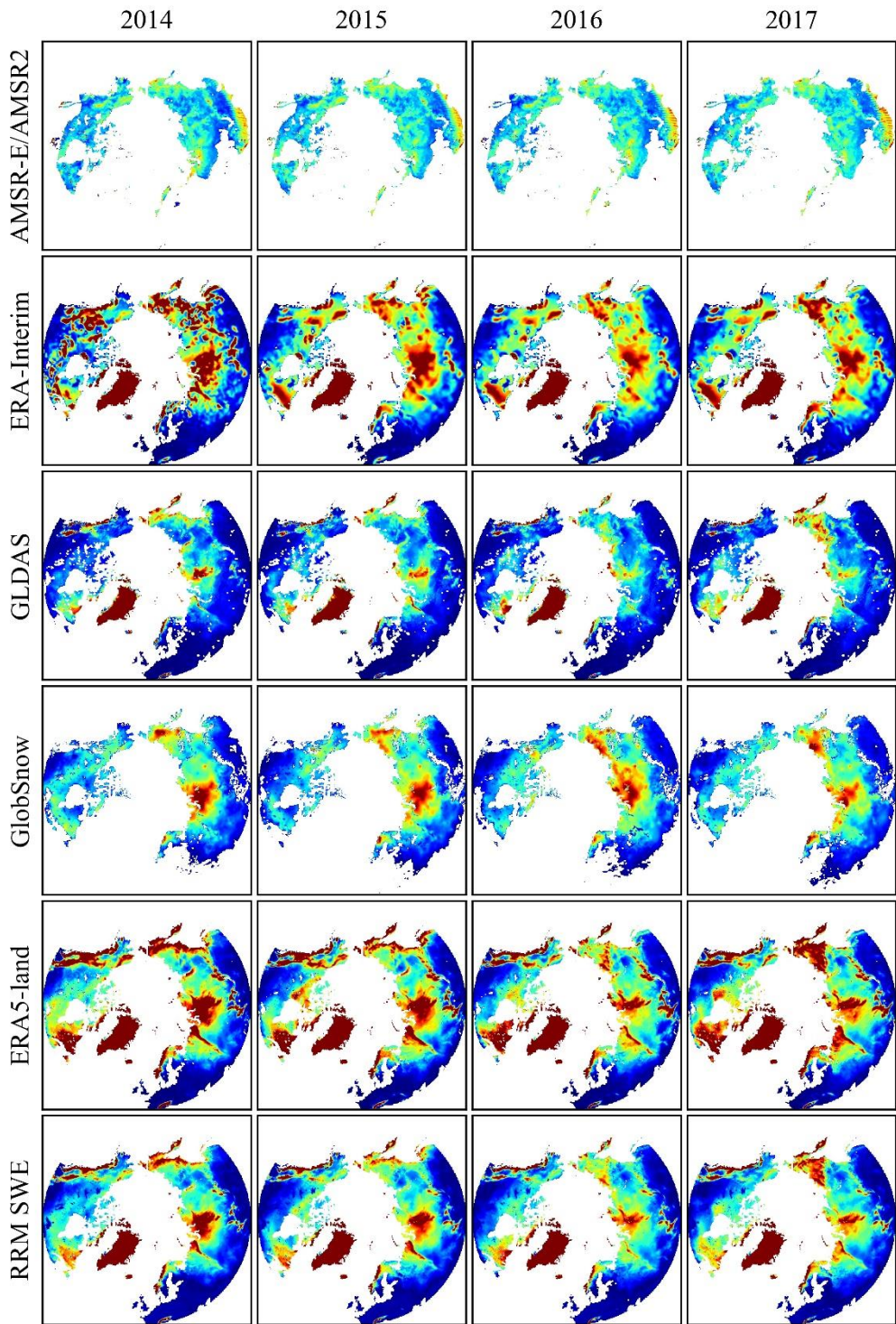
557

Figure 5: Comparison of the error between the RRM SWE and AMSR-E/AMSR2 SWE, ERA-Interim SWE, GLDAS SWE, GlobSnow SWE, and ERA5-land SWE at different altitudes (the abscissa represents the altitude gradient, and the ordinate represents different SWE datasets). The color bar indicates the error in each SWE dataset. The closer to red the color is, the higher the accuracy is. MAE: mean absolute error, RMSE: root mean square error, R: Pearson's correlation coefficient, R²: coefficient of determination).

558 **Table 3: Error list for the station data and RRM SWE product in different regions.**

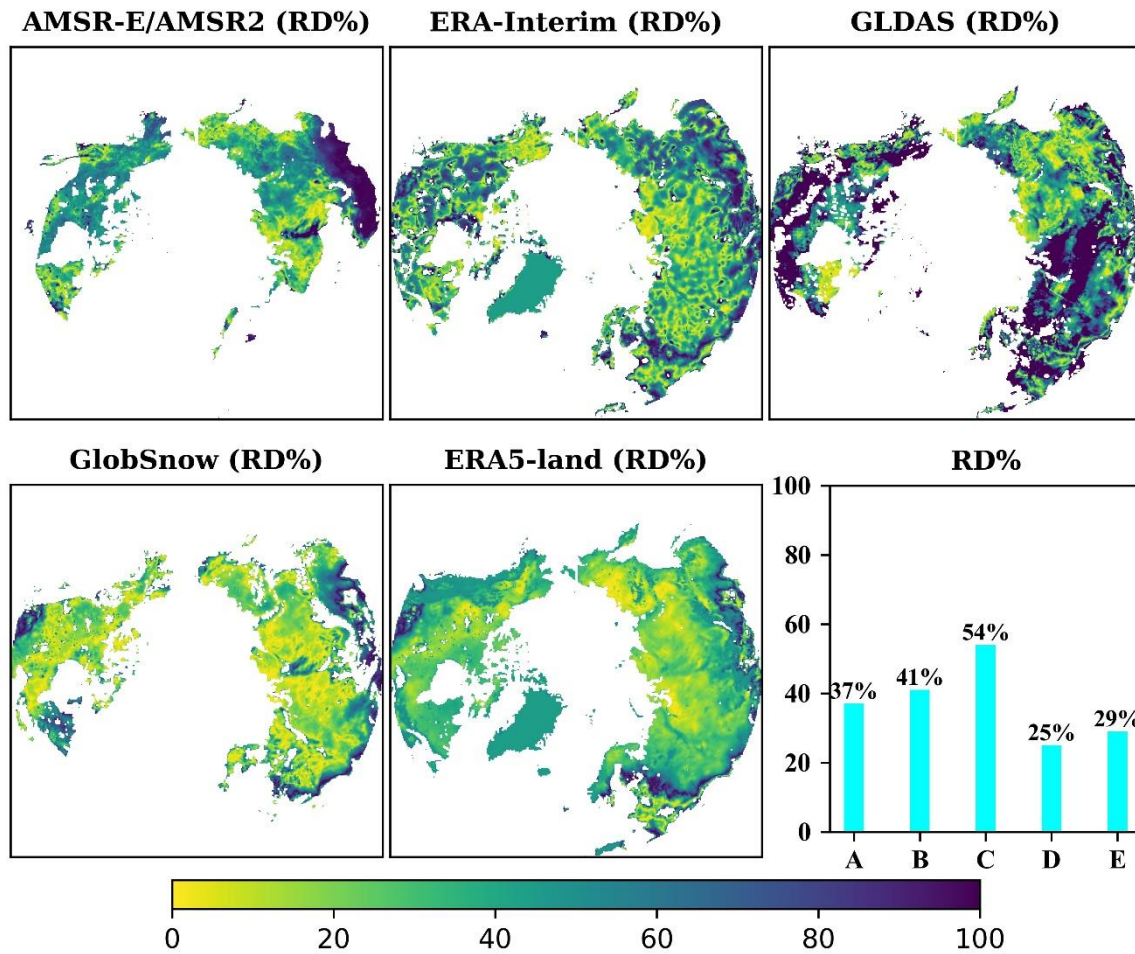
Region	MAE	RMSE (mm)	R	R²
Russia	0.20	26.39	0.89	0.79
Canada	0.23	29.31	0.87	0.76
Finland	0.21	25.29	0.89	0.79

559



561 **Figure 6: Comparison of the spatial distribution characteristics between the RRM SWE and AMSR-E/AMSR2 SWE, ERA-**
562 **Interim SWE, GLDAS SWE, GlobSnow SWE, and ERA5-land SWE (the four columns of images represent the comparison results**
563 **in 2014, 2015, 2016, and 2017, respectively).**

564



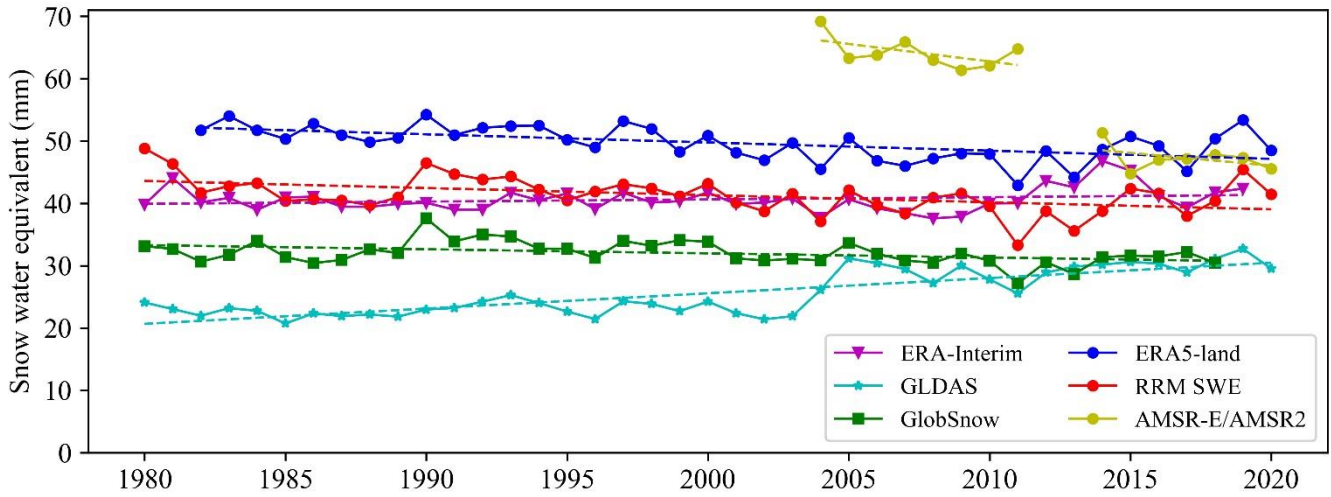
565

566 Figure 7: Temporal and spatial distributions of relative differences (RD%) between the RRM SWE and AMSR-E/AMSR2 SWE,

567 ERA-Interim SWE, GLDAS SWE, GlobSnow SWE, and ERA5-land SWE. Lower-right subgraph: Comparison of annual average

568 relative differences between the RRM SWE and AMSR2 SWE (A), ERA-Interim SWE (B), GLDAS SWE (C), GlobSnow SWE

569 (D), and ERA5-land SWE (E).



570

571

Figure 8: Annual variation tendency in the AMSR-E/AMSR2 SWE, ERA-Interim SWE, GLDAS SWE, GlobSnow SWE, ERA5-land SWE and RRM SWE products from 1979 to 2019 (the dotted line is the trend line calculated based on the Mann-Kendall method).

572

573

574

Table 4: Results of the Mann-Kendall trend test performed for various snow water equivalent products from 1979 to 2019.

Data	P value	Test value	Trend
AMSR-E/AMSR2	0.00	-3.26	Decreasing
ERA-Interim	0.27	1.08	No trend
GLDAS	7.29e-07	4.95	Increasing
GlobSnow	0.01	-2.54	Decreasing
ERA5-land	0.00	-3.43	Decreasing
RRM SWE	0.00	-3.00	Decreasing

*Significance level $\alpha = 0.05$